Biogeochemical Layering and Transformation of Particulate Organic Carbon in the Tropical Northwestern Pacific Ocean Inferred from $\delta^{13}C$

Authors

Detong Tian[1,3], Xuegang Li[1,2,3,4*], Jinming Song[1,2,3,4*], Jun Ma[1,2], Huamao Yuan[1,2,3,4], Liqin Duan[1,2,3,4]

Affiliations

[1]CAS Key Laboratory of Marine Ecology and Environmental Sciences, Institute of Oceanology, Chinese Academy of Sciences, Qingdao 266000, China

[2]Laboratory for Marine Ecology and Environmental Science, Qingdao Marine Science and Technology Center, Qingdao 266237, China

[3]University of Chinese Academy of Sciences, Beijing 100049, China

[4]Center for Ocean Mega-Science, Chinese Academy of Sciences, Qingdao 266000, China

Corresponding to: Xuegang Li (lixuegang@qdio.ac.cn) and Jinming Song (jmsong@qdio.ac.cn).

Abstract. Particulate organic carbon (POC) serves as the main carrier of the biological pump and determines its transmission efficiency, yet the transformation processes of POC remain incompletely understood. This study reports the vertical distribution of POC, dissolved inorganic carbon (DIC), δ^{13}C-POC, and δ^{13}C-DIC in the tropical Northwestern Pacific Ocean (TNPO). The research identified three distinct biogeochemical layers governing POC transformation: the POC rapid synthesis-degradation layer (RSDL, 0-300 m), the net degradation layer (NDL, 300-1,000 m), and the stable layer (SL, 1,000-2,000 m). From the top to the bottom of the RSDL, δ^{13}C-POC values decreased by an average of 2.23‰, while the carbon-to-nitrogen ratios (C:N) increased by an average of 2.3:1, indicating the selective degradation of POC. In the NDL, δ^{13}C-POC and δ^{13}C-DIC exhibited a significant negative correlation (r = 0.43, p < 0.05), indicating a net transformation of POC to DIC. In the SL, POC proved to be resistant to degradation, with POC exhibiting the highest C:N (15:1 on average) and the lowest δ^{13}C-POC values (average -27.71‰).

1 Introduction

As the most significant carbon reservoir on the earth's surface, the ocean absorbs about 2.6 billion tons of carbon dioxide (CO_2) from the atmosphere each year, accounting for 25% of global anthropogenic CO_2 emissions (Friedlingstein et al., 2023). After entering the ocean, CO_2 initially dissolves in seawater, forming dissolved inorganic carbon (DIC). Subsequently, phytoplankton and photosynthetic bacteria at the ocean surface convert it into organic carbon through photosynthesis. The majority of carbon in the ocean is in the form of DIC, constituting over 98% of the total carbon content, with the remaining 2%

34 existing as POC and dissolved organic carbon (DOC). ~~Despite being in minimal quantities,~~ Particulate

35 organic carbon (POC) can be transported to the deep ocean (> 1,000 m) through the biological pump and

36 buried for thousands of years. This process of carbon sequestration aids in the absorption of CO_2 by the

37 ocean, contributing to the regulation of atmospheric CO_2 levels (Longhurst and Glen Harrison, 1989;

38 Turner, 2015). Organic matter produced ~~from~~ in the euphotic layer is the primary food source for

39 heterotrophic communities in the dark ocean (Smith et al., 2008); once POC is exported from the euphotic

40 layer, microorganisms may rapidly utilize it, releasing DIC (Song, 2010).

41 Some studies have shown that unstable components such as proteins and carbohydrates in POC are

42 preferentially degraded by microorganisms (Eadie and Jeffrey, 1973). However, conducting detailed

43 quantitative analyses of each POC component in actual investigations is challenging, necessitating the

44 use of alternative indicators to demonstrate selective degradation. One generally accepted indicator is the

45 carbon-to-nitrogen ratios (C:N) due to inherent differences in the C:N of various compounds in POC

46 (Morales et al., 2021). Thus, changes in the C:N during degradation can signify the selective degradation

47 of POC. Nevertheless, the composition of POC is highly complex, and the C:N of its different

48 components are not absolute. For example, lipids typically have a higher C:N than proteins, but the

49 opposite can also occur (Sannigrahi et al., 2005; Hernes and Benner, 2002). Therefore, relying solely on

50 the C:N to reflect the selective degradation process of POC has significant limitations. ~~Although t~~The

51 vital activities of the microbial community in the dark ocean are predominantly driven by heterotrophic

52 respiration (Herndl et al., 2023), while many autotrophic organisms also use chemical energy to

53 synthesize POC. There is c~~C~~ompelling evidence ~~indicates~~ that chemoautotrophy plays a substantial role

54 in the fixation of DIC in the ~~minimum oxygen zone (OMZ)~~(Reinthaler et al., 2010) and the deeper ocean

55 (Passos et al., 2022; Walsh et al., 2009). Consequently, there is a continuous conversion of POC and DIC

56 throughout the ocean water column. Exploring the degradation and synthesis of POC in the ocean is

57 imperative to enhance our comprehension of the biological pump processes.

58 The DIC in seawater primarily occurs in four chemical forms: H_2CO_3, HCO_3^-, CO_3^{2-}, and CO_2. In

59 comparison, the composition of POC is more complex. POC comprises various organic compounds

60 originating from living organisms such as phytoplankton, zooplankton, and microorganisms. It also

61 encompasses fecal particles, cell fragments, and diverse organic substances from external sources. Only

62 a small fraction of the POC has been accurately identified in terms of molecular structures (Kharbush et

63 al., 2020). As the depth increases, the readily degradable components in POC are used up, leading to a

more intricate structure of the remaining POC through the transformation process. The remaining refractory POC is even more difficult to identify (Lee et al., 2000). Therefore, it becomes challenging to study the chemical characteristics of POC and its transformation process from itself. The δ^{13}C value is a crucial indicator that can reveal the origin, migration, and transformation of POC, making it ~~significantly~~ important in the investigation of the marine carbon cycle (Ding et al., 2020; Jeffrey et al., 1983). Compared with POC concentration, δ^{13}C-POC provides a more accurate reflection of the chemical properties of the POC pool and the migration and transformation processes of POC (Close and Henderson, 2020). Similarly, δ^{13}C-DIC can offer insights into important processes within the ocean carbon cycle. As POC settles, it undergoes a series of biogeochemical processes, including synthesis, degradation, and adsorption. Therefore, the isotope fractionation effect in POC is strong, resulting in significant differences in δ^{13}C-POC values at different depths. In contrast, the fractionation of δ^{13}C-DIC is subject to fewer influencing factors, and the DIC concentration in the ocean is notably high, thereby engendering minimal variability in δ^{13}C-DIC values across the ocean water column (Jeffrey et al., 1983). Therefore, δ^{13}C-DIC is more sensitive to the fractionation effect in the ocean carbon cycle. Even slight variations in the δ^{13}C-DIC values can reflect significant processes involved in the migration and transformation of POC (Quay and Stutsman, 2003). Through the analysis of δ^{13}C-POC and δ^{13}C-DIC values, we can enhance our comprehension of the intricate composition, transport, and alteration mechanism of POC, providing us with a more profound insight into the dynamic transformations within the ocean biological pump.

The tropical Northwestern Pacific Ocean (TNPO) is characterized by intricate current patterns and water mass distributions (Hu et al., 2015; Schönau et al., 2022), and it is also known for the highest surface seawater temperatures globally (Jia et al., 2018). High temperatures facilitate the respiration by heterotrophic organisms, promoting the formation of biological hotspots and ultimately enhancing material circulation and energy flow in the upper ocean (0-300 m) (Guo et al., 2023a; Iversen and Ploug, 2013). The air-sea interaction within the TNPO is highly dynamic, exhibiting a shift from being a carbon sink to a carbon source as it extends from higher to lower latitudes (Takahashi et al., 2009; Wu et al., 2005). The complex hydrological characteristics, rapid elemental cycle, and frequent air-sea exchange render the TNPO an ideal laboratory for exploring the ocean carbon cycle. In this research, we collected seawater and particulate matter samples at six stations in the core and boundary regions of the TNPO,

and the relationship between DIC, POC, and their stable carbon isotopes was comprehensively analyzed

to enhance our understanding of the POC transformation process and the ocean carbon cycle ~~process~~.

2 Sampling and Methods

The samples were collected in the TNPO during an expedition on R/V *Kexue* from 16 February~~March~~ to

12 April 2022. A total of 6 stations were set up: EQ-6 (150.99° E, 0.00° N, 1944 m), E142-3 (140.99° E,

12.01° N, 4091 m), E142-7 (140.99° E, 15.99° N, 4725 m), E142-11 (140.99° E, 20.00° N, 462 4m),

E142-13 (142.04° E, 0.00° N, 3382 m) and E142-19 (141.99° E, 6.01° N, 2580 m) (Fig. 1). The 12-L

Niskin bottles (KC-Denmark, Denmark) mounted on a Conductivity-Temperature-Depth (CTD, Sea-bird

SBE911, United States) rosette were used to obtain water samples from the vertical profile of 0-2,000 m

at each station for analysis of temperature, salinity, dissolved oxygen (DO), POC, δ^{13}C-POC, particulate

nitrogen (PN), DIC, δ^{13}C-DIC, and chlorophyll a (Chl-*a*). The specific sampling and analysis methods

are as follows.

Temperature and salinity: The temperature and salinity were measured by CTD ~~(Sea-bird SBE911, United States)~~ in situ ~~during sampling~~, with accuracies of ± 0.001 °C and ± 0.0003 S m^{-1}, respectively

(Ma et al., 2024).

DO: DO was determined in situ using the manual Winkler titration method, with a measurement

precision of ~~2.2 × 10^{-3}~~0.22 μmol L^{-1}. At each depth, we collected samples in 50 mL brown bottles, added

manganese sulfate and alkaline potassium iodide to fix the oxygen, then manually titrated the released

iodine with sodium thiosulfate using a calibrated burette to calculate DO concentrations (Bryan et al.,

1976; Zuo et al., 2018). The discrete DO samples were used to calibrate the DO concentration data

obtained by the CTD sensor.

POC, δ^{13}C-POC, and PN: Particle samples were obtained by filtering 2-5 L of seawater onto a GF/F

glass filter (0.7 μm, Whatman) that had been combusted in a muffle furnace (450 °C, 4 h) and acid-

soaked (0.5 M hydrochloric acid ~~(HCl)~~, 24 h). ~~The filter was treated with HCl to remove inorganic carbonates and oven-dried at 60°C.~~ After collection, samples were stored below -20 °C until laboratory

analysis. Before analysis, ~~T~~the filter was treated with concentrated hydrochloric acid~~HCl~~ to remove

inorganic carbonates and oven-dried at 60 °C. Afterward, POC, PN concentration, and δ^{13}C-POC

value~~s~~ were analyzed using an elemental analyzer and an isotope mass spectrometer (Thermo Fisher

Scientific Flash EA 1112 HT-Delta V Advantages, United States) with an accuracy of ± 0.8‰, ± 3‰

and ± 0.2‰, respectively. Blank filters were analyzed alongside samples and exhibited negligible

background levels for POC, PN, and δ^{13}C-POC value. Standard reference materials were used to calibrate

δ^{13}C and POC, PN measurements, including USGS64 (δ^{13}C = -40.8 ± 0.04‰, C% = 31.97%, N% =

18.65%, Indiana University), USGS40 (δ^{13}C = -26.39 ± 0.04‰, C% = 40.8%, N% = 9.52%, Geological

Survey, United States), and Urea #2a (δ^{13}C = -9.14 ± 0.02‰, C% = 20%, N% = 46.67%, Indiana

University). We implemented a quality control protocol by randomly inserting a certified reference

material after every 10 samples. The measured values of these reference materials were subsequently

plotted against the calibration curve to monitor and verify instrument stability throughout the analytical

process (Ma et al., 2021).

DIC and δ^{13}C-DIC: Sampling was performed using a 50 ml glass bottle. After the water sample

overflowed, 1 ml of the sample was taken out with a pipette and then fixed with saturated mercuric

chloride solution to remove the influence of biological activity. After collection, samples were stored in

refrigerator at 4 ℃ for later laboratory measurement of DIC concentration using a total DIC analyzer

(Apollo SciTech AS-C3, United States) with an accuracy of ± 0.1% (Ma et al., 2020). For calibration,

certified reference material (Batch 144, 2031.53 ± 0.62 μmol/kg) provided by the Scripps Institution of

Oceanography (University of California, San Diego) was used. δ^{13}C-DIC values automatic analysis was

performed using a Thermo Delta-V isotope ratio mass spectrometer (ThermoFisher Scientific MAT

253Plus, United States). For calibration, certified reference materials for δ^{13}C-DIC were used, including

GBW04498 (δ^{13}C = -27.28 ± 0.10‰), GBW04499 (δ^{13}C = -19.58 ± 0.10‰), and GBW04500 (δ^{13}C = -

4.58 ± 0.12‰), all provided by the Institute of Geophysical and Geochemical Exploration (Chinese

Academy of Geological Sciences). We inserted a reference standard every 10 samples, using its measured

values to verify instrument stability via the calibration curve.

Chl–a: 2 L of water sample after zooplankton removal was filtered onto pre-combusted (450 ℃, 5 h)

GF/F filters (0.7 μm, Whatman) and placed in the refrigerator at -20 ℃ before measurement. In the

laboratory, the filters were extracted with 90% acetone for 12-24 h, and the concentration was measured

using a fluorescence photometer (Turner Designs, United States) For calibration, Chl-a analytical

standard (purity ≥ 95.0%) provided by Sigma-Aldrich (SIAL, St. Louis, MO, United States) was used.

(Ma et al., 2020).

Data analysis was conducted using OriginPro 2021 (v9.8.0.200). Inter-group differences were assessed

151 using t-tests, with statistical significance defined as $p < 0.05$. Linear relationships between variables were

152 examined using least-squares regression, and correlation strength was reported as the Pearson correlation

153 coefficient (r). An $r > 0$ denotes a positive correlation, $r < 0$ a negative correlation, and $|r|$ closer to 1

154 indicates a stronger linear relationship.
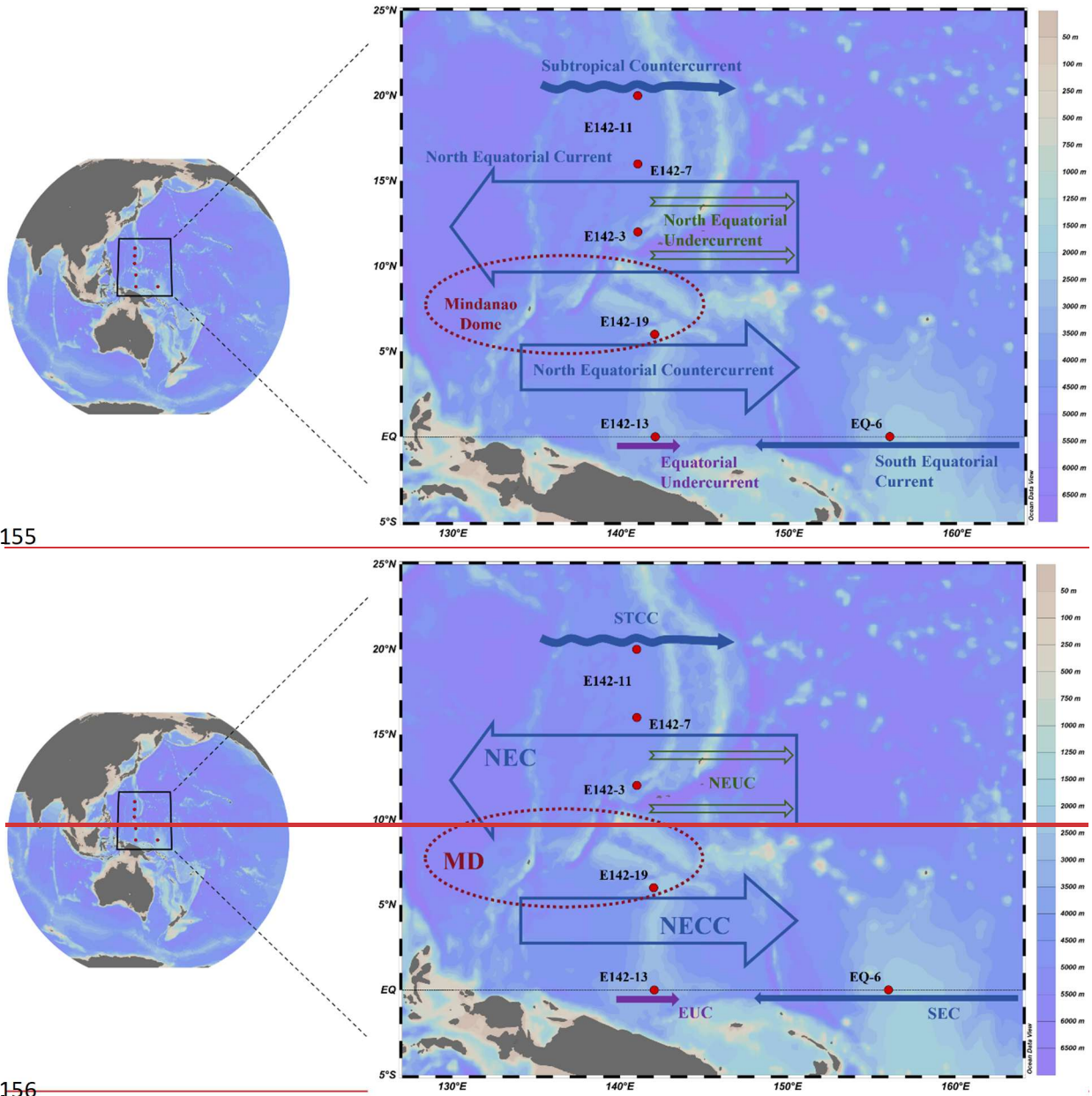
157 **Figure 1. TPWO sampling stations (red dots in the figure) and ocean current distribution. In the figure, blue**

158 **represents the ocean currents from the surface to the bottom of the thermocline, mainly Subtropical**

159 **Countercurrent~~STCC~~, North Equatorial Current~~NEC~~, North Equatorial Countercurrent~~NECC~~, and South**

160 **Equatorial Current~~SEC~~; green represents the ocean currents in the subthermocline, mainly North Equatorial**

161 **Undercurrent~~NEUC~~; purple represents the ocean currents from the bottom of the thermocline to the**

162 **subthermocline, mainly Equatorial Undercurrent~~EUC~~.**

3 Results and Discussion

3.1 Hydrological Characteristics

Except for station E142-11, the remaining five stations are all located at the Western Pacific Warm Pool (WPWP). The SST of the five stations in the warm pool area was higher, averaging 29.01 ± 0.67 ℃, while station E142-11 had a lower SST of 25.02 ℃. The strong seawater stratification in the study area restricted the movement of nutrient-rich water from the deep to the upper ocean, resulting in the region showing oligotrophic characteristics (Radenac et al., 2013). Therefore, the Chl-a concentration at the deep chlorophyll maximum layer depth (DCMD) was low, with an average of only 0.24 ± 0.04 µg L^{-1}. Based on the fluorescence intensity measured by the CTD in-situ fluorescence sensor, we calculated the ~~P~~primary ~~Production~~ production ~~Zone~~ zone ~~Depth~~ depth (PPZD), which is the depth where the fluorescence intensity drops to 10% of its maximum value above this depth (Owens et al., 2015). Additionally, the ~~Mixed~~ mixed ~~Layer~~ layer ~~Depth~~ depth (MLD) at each station was determined using the temperature threshold method (Table 1) (Thompson, 1976). The results indicate that the PPZD at each station is deeper than the MLD, suggesting that the POC generated at these stations does not undergo particularly complex physical mixing after its formation (Buesseler et al., 2020).

Table 1. ~~The w~~Water depth (WD), primary production zone depth (PPZD)~~the PPZD~~, mixed layer depth (MLD)~~the MLD~~, ~~the~~ deep chlorophyll maximum layer depth (DCMD), and the chlorophyll-a (Chl-a)~~Chl-a~~ concentration at DCMD for each station.

Station	Longitude °E	Latitude °N	WD m	PPZD m	MLD m	DCMD m	Chl-a µg L^{-1}
EQ-6	155.99	0.00	1944	129	65	50	0.31
E142-3	141.00	12.01	4091	216	102	140	0.19
E142-7	141.00	16.00	4725	204	68	150	0.25
E142-11	140.99	20.00	4624	203	42	90	0.21
E142-13	142.04	0.00	3382	165	45	90	0.25
E142-19	142.00	6.01	2580	170	109	100	0.21

Based on the relationship between potential temperature and salinity (θ-S) (Fig. 2), eight water masses in the study area were identified: North Pacific Tropical Surface Water (NPTSW), North Pacific Subsurface Water (NPSSW), North Pacific Subtropical Mode Water (NPSTMW), North Pacific Intermediate Water (NPIW), North Pacific Deep Water (NPDW), as well as Equatorial Surface Water (ESW), South Pacific Subsurface Water (SPSSW) and South Pacific Intermediate Water (SPIW) (Sun et al., 2008). In the upper ocean ~~(0-300 m)~~, we found that both NPTSSW and SPSSW exhibited high salinity

characteristics. The salinity of NPTSSW was distributed between 34.66 and 35.01, while the salinity of SPSSW was distributed between 35.15 and 35.65. In addition, as the water depth increased, the temperature of NPTSSW and SPSSW decreased significantly, with NPTSSW dropping from 27.18 ℃ to 16.21 ℃ and SPSSW dropping from 29.23 ℃ to 14.81 ℃. The representative water mass in the intermediate~~middle~~ ocean (300-1000 m) is NPIW, which is characterized by a rapid decrease in temperature (11.44-5.57 ℃) and a slight increase in salinity (~0.3) with increasing water depth. The representative water mass in the deep ocean ~~(1000-2000 m)~~ is NPDW, which has stable properties and slight ~~changes~~variations in salinity and temperature. Notably, the water mass distribution at station E142-19 is quite special. Ranging from the subsurface to the deep layer, the water mass properties of this station are relatively stable, showing low-salinity and low-temperature characteristics. This is attributed to the intrusion of both ~~North Pacific Intermediate Water (~~NPIW~~)~~ and ~~South Pacific Intermediate Water (~~SPIW~~)~~ into the station in the intermediate ocean layer~~mid-ocean region~~. Additionally, the station is situated within the Mindanao Dome~~MD~~ upwelling area, where strong upwelling transports low-temperature, low-salinity ~~North Pacific Deep Water (~~NPDW~~)~~ from the bottom to the upper layer, enhancing seawater exchange. Consequently, the water at station E142-19 comprises a mixture of diverse water masses ~~(MW)~~.
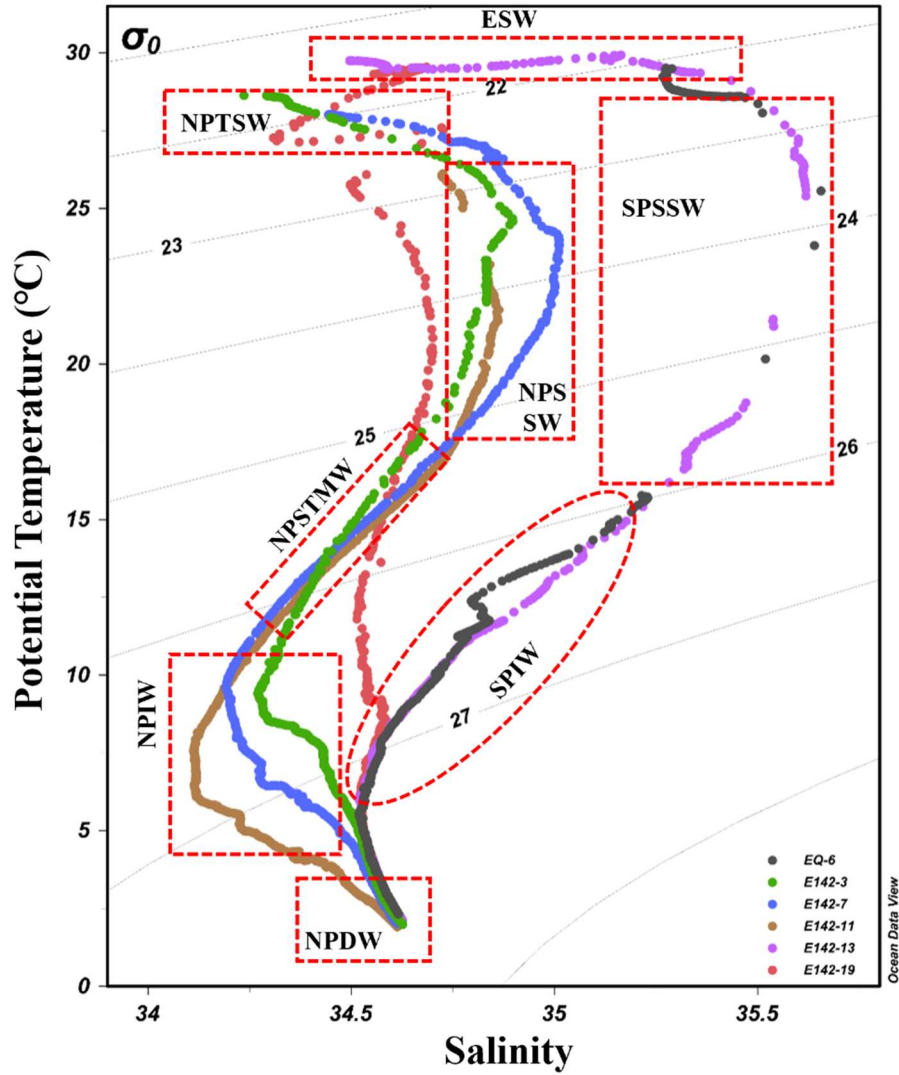
Figure 2. Relationship between potential temperature (θ) and salinity (S) at each sampling station. The water mass distribution is marked with a dotted line.

The study area is traversed by six major ocean currents: the South Equatorial Current ~~(SEC)~~, the North Equatorial Current ~~(NEC)~~, the North Equatorial Undercurrent ~~(NEUC)~~, the Subtropical Countercurrent ~~(STCC)~~, the Equatorial Undercurrent ~~(EUC)~~ and the North Equatorial Countercurrent ~~(NECC)~~ (Fig. 1). Among them, the South Equatorial Current ~~SEC~~ flows from east to west along the equator and is characterized by high temperature and low salinity, notably impacting station EQ-6. The North Equatorial Current~~NEC~~ is a major westward current in the study area, accompanied by a series of eastward undercurrents of the North Equatorial Undercurrent~~NEUC~~ in its lower part; stations E142-3 and E142-7 are mainly affected by them. The Subtropical Countercurrent~~STCC~~ is characterized by a multi-eddy structure that flows eastward in the subtropical region of the North Pacific and notably impacts station E142-11. The Equatorial Undercurrent ~~EUC~~ is a strong eastward current rich in oxygen

and nutrients, which are present in the subsurface layer of the equatorial Pacific, forming the main body of the thermocline of this area; station E142-13 is deeply affected by it. The North Equatorial Countercurrent NECC is an important current in the tropical Pacific equatorial current system, transporting warm pool water from the western Pacific to the eastern Pacific; Station E142-19 is mainly affected by it. Furthermore, the area features a substantial upwelling system known as the Mindanao Dome (MD), greatly impacting Station E142-19, situated southeast of the Mindanao DomeMD.

3.2 Vertical distribution characteristics of POC and δ^{13}C-POC

The average POC concentration from the surface to the deep chlorophyll maximum layer (DCM, 0-150 m) of the six stations was: E142-19 (34.12 ± 3.53 µg L^{-1}) > E142-13 (31.90 ± 3.19 µg L^{-1}) > EQ-6 (31.32 ± 5.27 µg L^{-1}) > E142-3 (27.77 ± 4.78 µg L^{-1}) > E142-7 (27.43 ± 1.35 µg L^{-1}) > E142-11 (26.81 ± 2.25 µg L^{-1}). Since the nutrient concentration in ESW and SPSSW is higher than that in NPTSW and NPTSSW, the The surface POC concentrations at stations E142-13 and EQ-6 were slightly higher than those at other stations, which can be attributed to higher nutrient levels in ESW and SPSSW than in NPTSW and NPTSSW. HoweverNotably, the surface POC concentration at station E142-19 was the highest among the six all stations, primarily due to the intense upwelling associated with the Mindanao Dome that brings nutrient-rich water to the surface because the robust upwelling of MD brought rich nutrients to the surface seawater, alleviating the nitrogen nutrient limitation of the surface water at this station (Gao et al., 2021).

The POC concentrations of at each all stations demonstrated a decreasing trend with increasing water depth and tended to remain stable in the deep ocean (> 1,000 m) (. The most significant drop in POC concentration occurred between the DCM and 600 m (Fig. 3). The seawater within this depth range was abundant in POC and also exhibited relatively high temperature and DO concentration, which likely enhanced the metabolic activities of heterotrophic organisms, thereby accelerating their utilization of POC (Iversen and Ploug, 2013; Sun et al., 2021). The aerobic degradation of POC led to a significantly consumedconsumption of DO, leading to decreased DO levels and the formation of an oxygen cline. Therefore, the change in DO in this water layer was consistent with the change of POC concentration (Fig. 3). It could be inferred that the rapid degradation of POC contributes to the accelerated formation of the oxygen cline. Since the microbial life activities below the oxygen cline were still active, leading to the continued consumption of DO through POC degradation, the DO cannot could not be replenished

in time. As a result, the low oxygen zone (where DO < 100 μmol L^{-1}) exists~~emerged~~ in the ~~intermediate~~middle ocean at all stations (Fig. 3). However, the hypoxic conditions observed at station E142-13 were comparatively less pronounced than those observed at other stations (Fig. 3). This can be attributed to the consistent transport of oxygen and nutrient-rich seawater by the Equatorial Undercurrent~~EUC~~ to this station, facilitating oxygen replenishment and mitigating deoxygenation (Brandt et al., 2021).
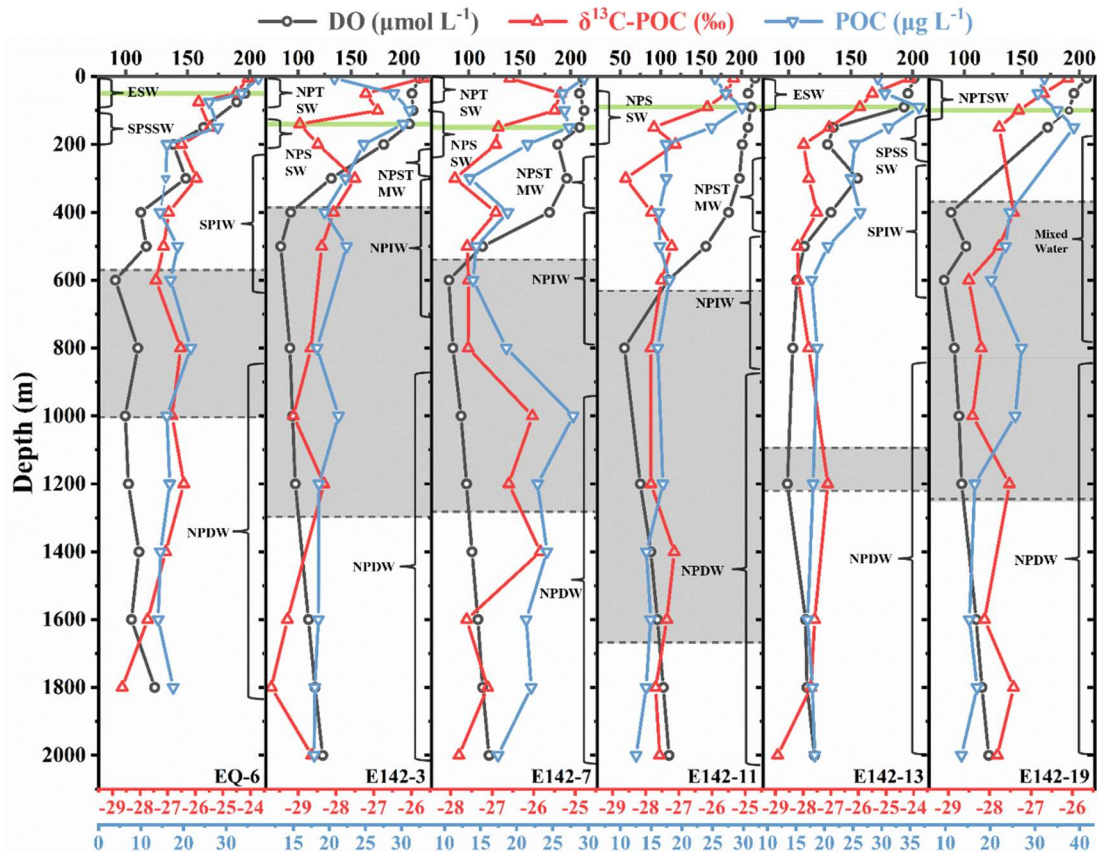
Figure 3. Vertical distribution of DO concentration, δ¹³C-POC values, and POC concentration at each sampling station. The gray area marks the hypoxic zone with DO = 100 μmol L^{-1} as the boundary. The green line represents the DCM depth.

The vertical distribution of δ¹³C-POC values closely resembles that of POC concentration (Figs. ~~2, 3a~~3, 4a)~~. This similarity suggests~~suggesting that specific δ¹³C-enriched components may be preferentially degraded during POC degradation. Although the molecular composition of oceanic POC cannot be fully identified, it is generally understood to primarily consist of lipids, amino acids, carbohydrates, nucleic acids, and a small number of heterogeneous components (Kharbush et al., 2020). The metabolic activity of amino acids and carbohydrates is higher than lipids, leading microorganisms to preferentially use these compounds as energy sources, enriching lipids in POC (Hwang et al., 2006; Jeffrey et al., 1983). Previous

studies have reported that during the degradation of POC, the carbon isotope fractionation characteristics of amino sugar monomers closely align with changes in δ^{13}C-POC values (Guo et al., 2023b). Moreover, several studies have highlighted that the carbon isotopic composition of lipid monomers does not exhibit significant depletion during POC degradation; in fact, it may even show a trend of enrichment (Close et al., 2014; Häggi et al., 2021). These observations further indicate the preferential degradation of amino acids and carbohydrates in POC. On the other hand, compared with lipids, amino acids and carbohydrates exhibit higher δ^{13}C values (Hayes, 1993; Hwang and Druffel, 2003; Schouten et al., 1998). When large quantities of amino acids and carbohydrates undergo selective degradation, the residual POC will show low δ^{13}C value characteristics. Therefore, as POC is continuously consumed in the water column, the δ^{13}C-POC values will gradually decrease. In addition, lipids have a low nitrogen content in comparison to amino acids and carbohydrates, leading to a relatively high C:N (Morales et al., 2021). Our findings demonstrated a strong negative correlation between δ^{13}C-POC values and C:N (Fig. 4b), which implied that as the water depth increases, δ^{13}C-POC values decreases while the C:N in the remaining POC increases. This suggests that selective degradation of POC occurs, during which amino acids and carbohydrates in the POC were are preferentially removed, resulting in a relative increase in the proportion of lipids in the remaining POC (Druffel et al., 2003; Guo et al., 2023a).

However, significant differences were observed among sampling stations in the relationships between δ^{13}C-POC value and POC concentration, as well as between δ^{13}C-POC value and C:N (Fig. S1). Among them, the EQ-6 station exhibited the most distinct regression trends. Located within the South Equatorial Current regime, where the water column is stable and strongly stratified, this station showed strong correlations ($p < 0.05$) between δ^{13}C-POC value and both POC concentration and C:N, indicating that degradation-dominated isotopic fractionation processes are prominent in this region (Tuchen et al., 2024). At station E142-13, under the influence of the Equatorial Undercurrent, continuous nutrient supply and an active biological pump created a marked gradient in POC content and composition between surface and subsurface waters (Brandt et al., 2021). As a result, significant correlations ($p < 0.05$) were also observed between δ^{13}C-POC value and both POC concentration and C:N. In contrast, at station E142-19, located in the Mindanao Dome upwelling region, the correlation between δ^{13}C-POC value and POC concentration was not significant ($p > 0.05$). This may be attributed to the upward transport of deep nutrients and the resuspension or entrainment of aged POC, leading to heterogeneous POC sources and ages in the water column, which diluted the isotopic fractionation signal associated with degradation

292 (Gao et al., 2021). Nevertheless, δ¹³C-POC at this station still exhibited a significant negative correlation

293 with C:N (p < 0.05), indicating the persistence of δ¹³C enrichment resulting from organic matter

294 degradation (Guo et al., 2023b). Moreover, although stations E142-3, E142-7, and E142-11 are located

295 within the same water mass regime (Fig. 2), their δ¹³C-POC value correlations with POC concentration

296 and C:N differed. At station E142-7, no significant correlation was found between δ¹³C-POC value and

297 C:N (p > 0.05). In contrast, stations E142-3 and E142-11 exhibited significant negative correlations

298 between δ¹³C-POC value and C:N (p < 0.05), likely due to stepwise degradation processes driven by

299 water column stratification. These two stations are probably situated at the edges or transition zones of

300 the water mass, where pronounced stratification limits vertical mixing, thereby creating stronger vertical

301 gradients in POC degradation and leading to the observed negative correlations (Close et al., 2014; Häggi

302 et al., 2021). In comparison, station E142-7 may be located near the water mass core, where enhanced

303 mixing results in a narrower vertical range of C:N (Fig. S1), suggesting a more uniform POC composition

304 throughout the water column. This homogeneity reduces spatial variability in degradation, thus

305 weakening the coupling between δ¹³C-POC value and C:N (Meyers, 1997).

306 In addition, it is noteworthy that in the upper ocean (0-300 m), although there is a significant negative

307 correlation between δ¹³C-POC values and C:N ratios (p < 0.05), no significant correlation is observed

308 between δ¹³C-POC values and POC concentration (p > 0.05) (Fig. 4a). This suggests that the fractionation

309 of δ¹³C-POC at this depth layer is not entirely controlled by selective degradation. Photosynthesis exerts

310 a certain influence on the fractionation of δ¹³C-POC within this depth range, primarily manifested as an

311 increase in photosynthetic carbon isotope fractionation with depth, leading to a decrease in δ¹³C-POC

312 values. In a study conducted in the subtropical North Atlantic, the photosynthetic carbon isotope

313 fractionation increased by 5.6‰ from the upper to the lower euphotic zone, while the δ¹³C values of the

314 photosynthetic product, phytol, decreased by 6.3‰ (Henderson et al., 2024). Therefore, although the

315 process of selective degradation significantly affects the fractionation of δ¹³C-POC, it is still necessary

316 to consider the regulatory effects of other processes in certain unique marine environments.

317

318
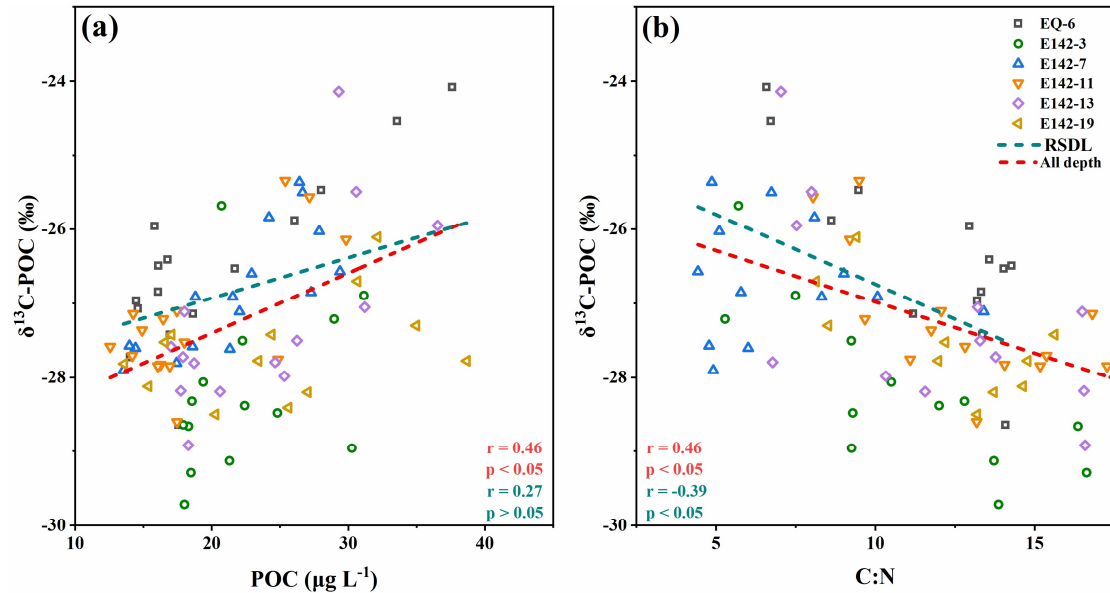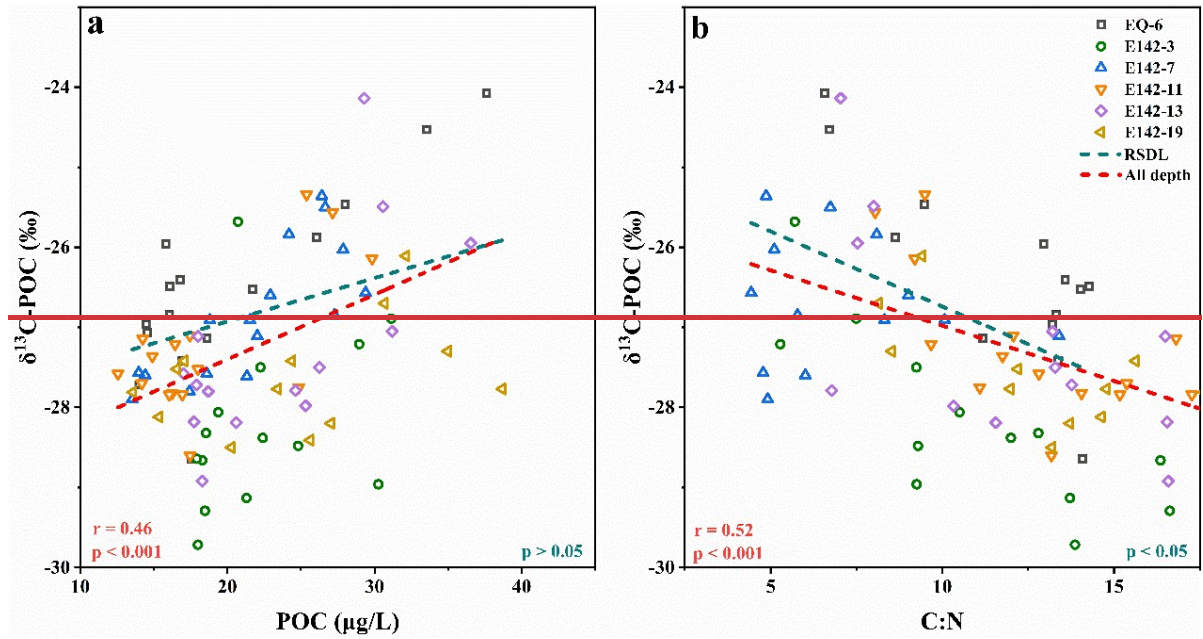
Figure 4. (a) Relationship between δ^{13}C-POC values and POC concentration; (b) Relationship between δ^{13}C-POC values and C:N. Red and green lines indicate regressions for the full water column and the rapid synthesis–degradation layer, respectively.

3.3 Vertical distribution characteristics of DIC and δ^{13}C-DIC

Among the six stations, only the equatorial stations E143-13 and EQ-6 exhibited average upper DIC concentrations exceeding 2000 μmol kg^{-1}, with values of 2036 and 2054 μmol kg^{-1}, respectively. This phenomenon can be attributed to the fact that the surface water masses at these stations are composed of high-temperature and high-salinity ESW (Fig. 2). Although high temperatures generally hinder the dissolution of CO_2, they can accelerate the rate of CO_2 release by heterotrophic organisms. Meanwhile,

high salinity increases the ionic strength and buffering capacity of seawater, promoting DIC

accumulation (Zeebe and Wolf-Gladrow, 2001). These factors collectively contribute to the high DIC

concentrations observed in the surface layers of these two stations. The average upper DIC concentration

at station E142-19 was the next highest, reaching 1992 μmol kg^{-1}. This is due to upwelling at this station,

which transports deep, high-DIC seawater to the intermediate~~middle~~ ocean. Consequently, this station

also recorded the highest average intermediate~~mid-layer~~ DIC concentration among the six stations, at

2184 μmol kg^{-1}. Furthermore, since stations E142-3, E142-7, and E142-11 are predominantly influenced

by the same water mass across all depths, their DIC concentrations are relatively similar at each depth

(Fig. 5). The average DIC concentrations of all six stations in the upper ocean, intermediate~~middle~~ ocean,

and deep ocean were 2004 ± 65, 2147 ± 35, and 2234 ± 26 μmol kg^{-1}, respectively. There was a significant

increase in DIC concentration from the upper to the deep ocean (Fig. 5). In the upper ocean, DIC

concentrations are lower due to photosynthetic uptake, whereas the decomposition of POC at

intermediate depths releases inorganic carbon, causing elevated DIC levels with ~~Affected by~~

~~photosynthesis, DIC increases gradually in the upper ocean. In contrast, in the middle ocean, the rapid~~

~~decomposition of POC released a large amount of inorganic carbon, causing a rapid increase in DIC~~

~~throughout the water column. Then~~depth. I~~,~~ in the deep ocean, a small amount of POC may still degrade,

and, along with the release of DIC driven by decreasing carbonate saturation, contributes to a gradual

further increase in DIC concentrations.~~a small amount of POC continues to degrade, while the release of~~

~~DIC due to decreasing carbonate saturation with depth contributes to a gradual increase in DIC~~

~~concentration within this layer.~~

Moreover, we observed surface δ^{13}C-DIC values ranging from -0.55 to 0.45‰ (average 0.12‰) in the

research region, which is significantly lower than those reported in studies conducted in the Pacific region

in the 1990s (Quay et al., 2017; Quay and Stutsman, 2003). This suggests that the ocean has absorbed

more anthropogenic CO_2 ~~as atmospheric CO₂ concentrations have increased~~ over the years. The surface

δ^{13}C-DIC value of station E142-11 was the lowest among the six stations, only -0.55‰, while the surface

δ^{13}C-DIC value of station EQ-6 was the highest ~~among the six stations~~, reaching 0.45‰. This is because

station E142-11 was located at the strongest atmospheric CO_2 net sink area, while station EQ-6 was

located at the atmospheric CO_2 net source area (Zhong et al., 2022). The sea-air exchange at station

E142-11 was sufficient, leading to a lower δ^{13}C-DIC value in its surface water, as it was more likely to

reach isotopic equilibrium with atmospheric CO_2. In contrast, the surface water of station EQ-6 was more

susceptible to seawater mixing and biological primary production influences. The higher δ^{13}C-DIC values observed in the surface water of station EQ-6 can be attributed to the isotope fractionation caused by the consumption of a substantial amount of CO_2 by biological primary production (Quay et al., 2003). In analyzing the vertical distribution of δ^{13}C-DIC, the findings revealed a pronounced ~~rapid~~ decrease in δ^{13}C-DIC values at each station (Fig. 5), consistent with the δ^{13}C-POC variations observed~~mirroring the decline seen in δ^{13}C-POC values~~ in the upper ocean ~~(0–300 m)~~ (Figs~~.~~ ~~4, 5d~~6d). Within this depth range, the average decrease in δ^{13}C-POC values was 2.23‰, while the average decrease of δ^{13}C-DIC values was 0.30‰, with δ^{13}C-DIC reaching its minimum value in the subsurface. However, in the intermediate~~middle~~ ocean layer ~~(300–1,000 m)~~, unlike δ^{13}C-POC, δ^{13}C-DIC values increased first and then stabilized (Fig. 5). Therefore, distinct differences exist in the overall change trends of δ^{13}C-DIC values and δ^{13}C-POC values in the ocean water column. Since the mutual conversion between POC and DIC was ongoing, this conversion process will inevitably cause changes in δ^{13}C-POC and δ^{13}C-DIC. Generally, the variation range of δ^{13}C-POC values was more significant than that of δ^{13}C-DIC values, indicating the more complex biogeochemical processes experienced by POC (Meyer et al., 2016; Schmittner et al., 2013). This difference is also partly due to the much larger size of the DIC pool compared to the POC pool (Jeffrey et al., 1983). The high DIC concentration in the ocean buffers its isotopic variability, resulting in minimal changes in δ^{13}C-DIC values across the water column, whereas the smaller POC pool is more sensitive to localized biogeochemical processes, leading to greater variability in δ^{13}C-POC values.

377
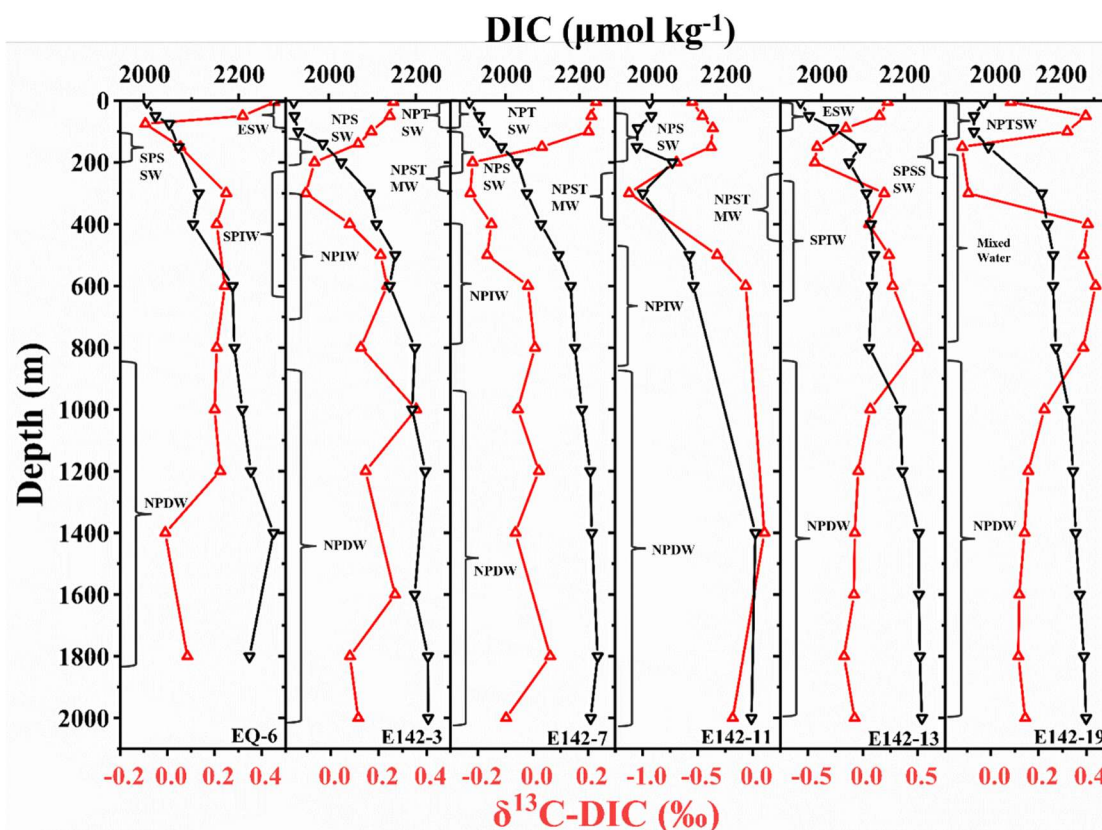
Figure 5. Vertical distribution of DIC concentration and δ¹³C-DIC values at each sampling station. The black line represents DIC, and the red line represents δ¹³C-DIC.

3.4 Transformation characteristics of POC in different water layers

According to the distribution characteristics of δ^{13}C-POC and δ^{13}C-DIC values, we divided the ocean water column into three biogeochemical layers: the POC rapid synthesis-degradation layer (RSDL, 0-300 m), the net degradation layer (NDL, 300-1,000 m) and the stable layer (SL, 1,000-2,000 m). Within the RSDL, POC undergoes concurrent synthesis and degradation (Calbet and Landry, 2004)POC was rapidly degraded while being synthesized. The synthesis of POC likely exceeded its degradation from the surface to the DCM layer, while the degradation of POC appeared to dominate below the DCM. In this layer, the δ^{13}C-POC values and C:N exhibited a pronounced negative correlation, while no significant correlation is observed between δ^{13}C-POC values and POC concentration ($p > 0.05$) (Figs. 4a, 6a). Therefore, the rapid decrease of δ^{13}C-POC values in this layer was dominated by the selective degradation of POC and by photosynthesis. Both δ^{13}C-POC and δ^{13}C-DIC values decrease with increasing depth in the RSDL (Figs. 3, 5), and they exhibit a significant positive correlation within this layer (Fig. 6d). Although the degradation of POC typically lowers the δ^{13}C value of DIC, as the δ^{13}C value of POC is lower than that of DIC, the significant decline in δ^{13}C-DIC values observed in the RSDL,

when considering the substantial difference in magnitude between the POC pool and the DIC pool, suggests the influence of additional processes. Specifically, the phytoplankton and photosynthetic bacteria in the upper ocean tended to use the light $^{12}CO_2$ in the seawater for photosynthesis; thus the $\delta^{13}C$-DIC values of the near surface ocean at all stations was were relatively high. However, light intensity diminishes with increasing depth, which is unfavorable for photosynthesis. This leads to the accumulation of $^{12}CO_2$ produced by the respiration of heterotrophic communities. Consequently, the $\delta^{13}C$-DIC values in this layer steadily declined with depth (Ge et al., 2022). In the NDL, sunlight was extremely weak, and photosynthesis was nearly absent. Heterotrophic communities dominate, leading to a continuous decrease in POC concentration and a corresponding increase in DIC concentration (Figs. 3, 5). Generally, the degradation of POC would be expected to lower the $\delta^{13}C$ value of DIC. However, in this layer, $\delta^{13}C$-POC values showed a significant negative correlation with both C:N and $\delta^{13}C$-DIC values (Fig. 6b, e), indicating the influence of additional processes on $\delta^{13}C$-DIC fractionation. The NDL often encompasses low-oxygen zones (Fig. 3), which are known to favor the activity of chemoautotrophic microorganisms. Compared to aerobic environments, the energy required for microorganisms to fix inorganic carbon into organic carbon is lower under low-oxygen conditions (Hugler and Sievert, 2011; Mccollom and Amend, 2005). During this process, chemoautotrophic microorganisms preferentially utilize lighter ^{12}C isotopes, leading to the enrichment of $\delta^{13}C$ in the remaining DIC pool. This microbial activity may explains explain the observed increase in $\delta^{13}C$-DIC values in the NDL. In the SL, the POC concentration remained consistently low. $\delta^{13}C$-POC values did not correlate significantly with either C:N or $\delta^{13}C$-DIC (Fig. 6c, f). This was because the easily degradable components in POC had been completely consumed in the RSDL and NDL, and the remaining components were relatively refractory. As a result, the conversion of POC to DIC was rare in SL, leading to an absence of a clear link between $\delta^{13}C$-POC and $\delta^{13}C$-DIC.
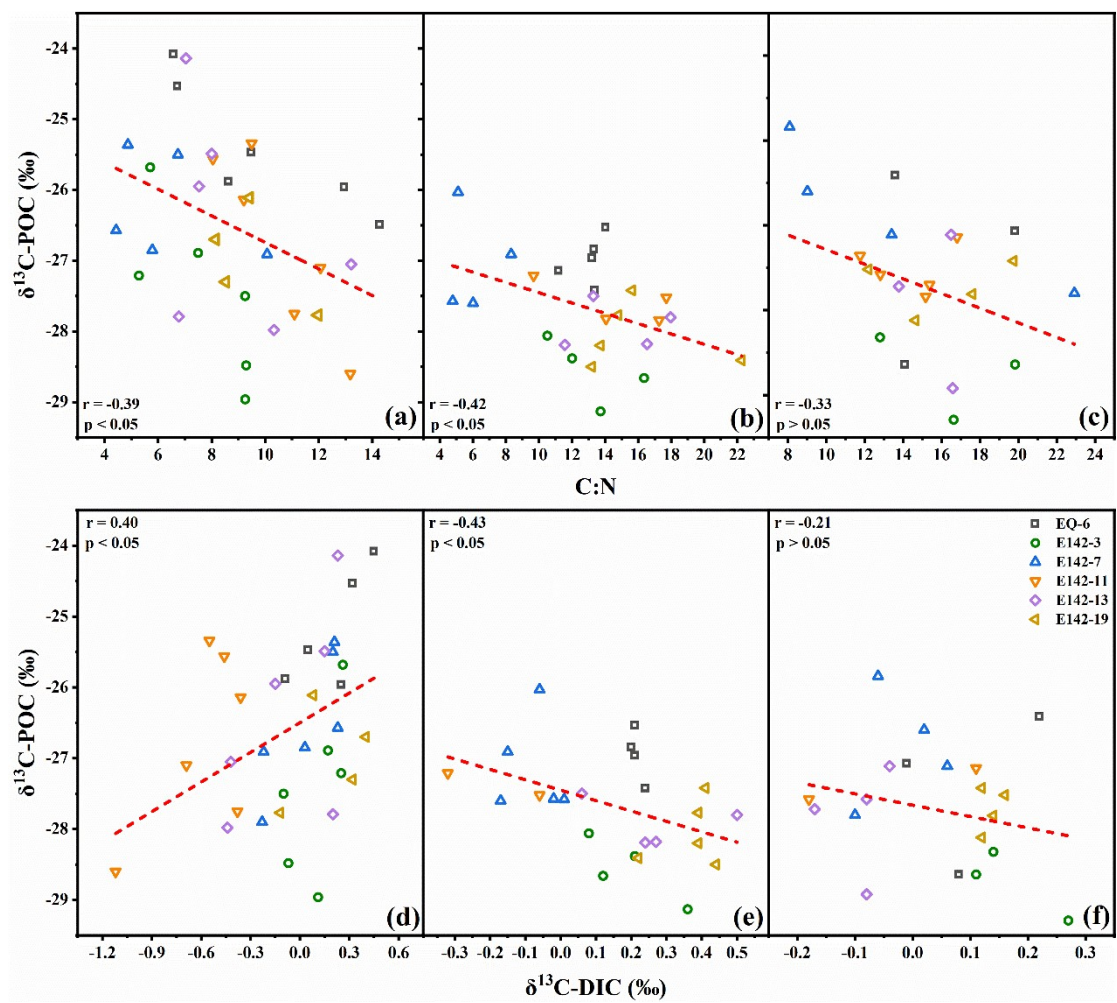
417
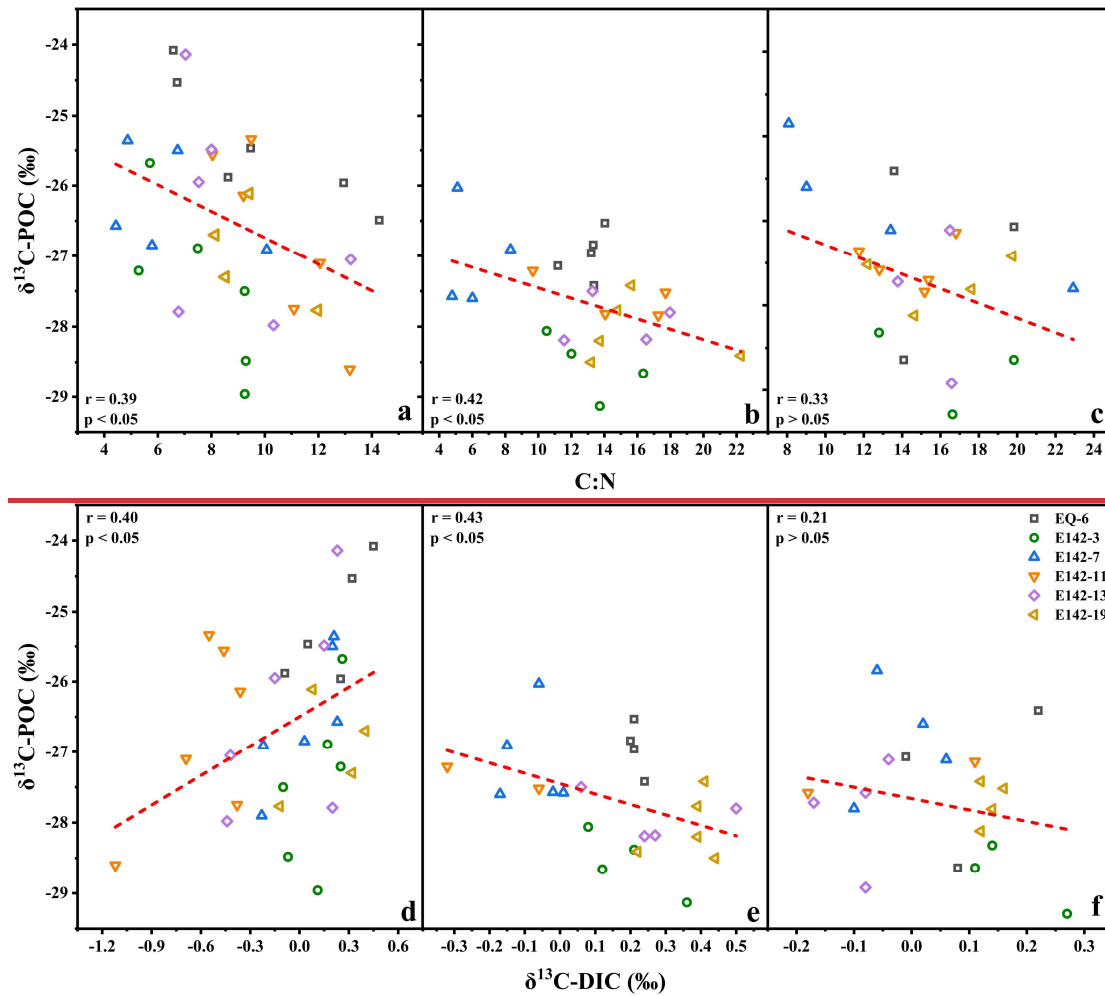
Figure 6. Relationships between δ^{13}C-POC and C:N at different depths: (a) 0-300 m, (b) 300-1,000 m, (c) 1,000-2,000 m, and between δ^{13}C-POC and δ^{13}C-DIC at different depths: (d) 0-300 m, (e) 300-1,000 m, (f) 1,000-2,000 m.

4 Conclusions

In general, this study investigated the transformation characteristics of POC in the tropical northwest Pacific Ocean based on the δ^{13}C perspective. Our findings revealed three distinct stages of POC behavior in the ocean: rapid synthesis-degradation, net degradation, and stable existence. Below the RSDL, the selective degradation of POC dominated the changes in δ^{13}C-POC. The C:N ratio data in RSDL and NDL indicate an increase in the proportion of refractory lipids in POC, relative to more labile components such as amino acids and carbohydrates. Consequently, in the SL, POC was found to be stable with a slow degradation rate. The fractionation of δ^{13}C-DIC in the ocean is influenced by both the production and degradation processes of POC. Within the RSDL, δ^{13}C-DIC fractionation is predominantly governed by

primary production, whereas within the NDL and SL, it is primarily influenced by the degradation process of POC.

Although we utilized δ^{13}C-POC and δ^{13}C-DIC to assess the overall transformation characteristics of POC, the specific synthesis and decomposition ratios of POC are still challenging to determine. Further research is needed on the monomer carbon isotopic composition of POC (lipids, amino acids, etc.) to enhance our understanding of the transformation process of POC.

Data Availability. The data files used in this paper are available at (Tian et al., 2024).

Competing interest. The authors declare that they have no conflict of interest.

Author contribution. Detong Tian: Investigation, Data Curation, Writing-original draft. Xuegang Li and Jinming Song: Conceptualization, Funding acquisition, Writing-review & editing. Jun Ma, Funding acquisition. Huamao Yuan, Liqin Duan: Writing - Review & Editing.

Acknowledgments. This work was supported by the National Key Research and Development Program (grant no. 2022YFC3104305), National Natural Science Foundation of China (grant nos.42176200, 42206135); Laoshan Laboratory (grant nos. LSKJ202204001, LSKJ202205001). We appreciate the crews of the R/V *Kexue* for sampling assistance during the cruise of NORC2021-09 supported by the National Natural Science Foundation of China (project no. 42049909).

References

Brandt, P., Hahn, J., Schmidtko, S., Tuchen, F. P., Kopte, R., Kiko, R., Bourlès, B., Czeschel, R., and Dengler, M.: Atlantic Equatorial Undercurrent intensification counteracts warming-induced deoxygenation, Nat. Geosci., 14, 278-282, http://doi.org/10.1038/s41561-021-00716-1, 2021.

Bryan, J. R., Rlley, J. P., and Williams, P. J. L.: A winkler procedure for making precise measurements of oxygen concentration for productivity and related studies, Journal of Experimental Marine Biology and Ecology, 21, 191-197, http://doi.org/10.1016/0022-0981 (76)90114-3, 1976.

Buesseler, K. O., Boyd, P. W., Black, E. E., and Siegel, D. A.: Metrics that matter for assessing the ocean biological carbon pump, Proc Natl Acad Sci U S A, 117, 9679-9687, http://doi.org/10.1073/pnas.1918114117, 2020.

Calbet, A. and Landry, M. R.: Phytoplankton growth, microzooplankton grazing, and carbon cycling in marine systems, Limnology and Oceanography, 49, 51-57, http://doi.org/10.4319/lo.2004.49.1.0051, 2004.

Close, H. G. and Henderson, L. C.: Open-Ocean Minima in $\delta^{13}C$ Values of Particulate Organic Carbon in the Lower Euphotic Zone, Front. Mar. Sci., 7, http://doi.org/10.3389/fmars.2020.540165, 2020.

Close, H. G., Wakeham, S. G., and Pearson, A.: Lipid and ^{13}C signatures of submicron and suspended particulate organic matter in the Eastern Tropical North Pacific: Implications for the contribution of Bacteria, Deep Sea Res. Part I Oceanogr. Res. Pap., 85, 15-34, http://doi.org/10.1016/j.dsr.2013.11.005, 2014.

Ding, L., Qi, Y., Shan, S., Ge, T., Luo, C., and Wang, X.: Radiocarbon in Dissolved Organic and Inorganic Carbon of the South China Sea, J. Geophys. Res. Oceans, 125, http://doi.org/10.1029/2020jc016073, 2020.

Druffel, E. R. M., Bauer, J. E., Griffin, S., and Hwang, J.: Penetration of anthropogenic carbon into organic particles of the deep ocean, Geophys. Res. Lett., 30, http://doi.org/10.1029/2003gl017423, 2003.

Eadie, B. J. and Jeffrey, L. M.: $\delta^{13}C$ analyses of oceanic particulate organic matter, Mar. Chem., 1, 199-209, http://doi.org/10.1016/0304-4203 (73)90004-2, 1973.

Friedlingstein, P., O'Sullivan, M., Jones, M. W., Andrew, R. M., Bakker, D. C. E., Hauck, J., Landschützer, P., Le Quéré, C., Luijkx, I. T., Peters, G. P., Peters, W., Pongratz, J., Schwingshackl, C., Sitch, S., Canadell, J. G., Ciais, P., Jackson, R. B., Alin, S. R., Anthoni, P., Barbero, L., Bates, N. R., Becker, M., Bellouin, N., Decharme, B., Bopp, L., Brasika, I. B. M., Cadule, P., Chamberlain, M. A., Chandra, N., Chau, T.-T.-T., Chevallier, F., Chini, L. P., Cronin, M., Dou, X., Enyo, K., Evans, W., Falk, S., Feely, R. A., Feng, L., Ford, D. J., Gasser, T., Ghattas, J., Gkritzalis, T., Grassi, G., Gregor, L., Gruber, N., Gürses, Ö., Harris, I., Hefner, M., Heinke, J., Houghton, R. A., Hurtt, G. C., Iida, Y., Ilyina, T., Jacobson, A. R., Jain, A., Jarníková, T., Jersild, A., Jiang, F., Jin, Z., Joos, F., Kato, E., Keeling, R. F., Kennedy, D., Klein Goldewijk, K., Knauer, J., Korsbakken, J. I., Körtzinger, A., Lan, X., Lefèvre, N., Li, H., Liu, J., Liu, Z., Ma, L., Marland, G., Mayot, N., McGuire, P. C., McKinley, G. A., Meyer, G., Morgan, E. J., Munro, D. R., Nakaoka, S.-I., Niwa, Y., O'Brien, K. M., Olsen, A., Omar, A. M., Ono, T., Paulsen, M., Pierrot, D., Pocock, K., Poulter, B., Powis, C. M., Rehder, G., Resplandy, L., Robertson, E., Rödenbeck, C., Rosan, T. M., Schwinger, J., Séférian, R., Smallman, T. L., Smith, S. M., Sospedra-Alfonso, R., Sun, Q., Sutton, A. J., Sweeney, C., Takao, S., Tans, P. P., Tian, H., Tilbrook, B., Tsujino, H., Tubiello, F., van der Werf, G. R., van Ooijen, E., Wanninkhof, R., Watanabe, M., Wimart-Rousseau, C., Yang, D., Yang, X., Yuan, W., Yue, X., Zaehle, S., Zeng, J., and Zheng, B.: Global Carbon Budget 2023, Earth Syst. Sci. Data, 15, 5301-5369,

491   http://doi.org/10.5194/essd-15-5301-2023, 2023.

492   Gao, W., Wang, Z., Li, X., and Huang, H.: The increased storage of suspended particulate matter in the
493   upper water of the tropical Western Pacific during the 2015/2016 super El Niño event, J. Oceanol.
494   Limnol., 39, 1675-1689, http://doi.org/10.1007/s00343-021-0362-0, 2021.

495   Ge, T., Luo, C., Ren, P., Zhang, H., Fan, D., Chen, H., Chen, Z., Zhang, J., and Wang, X.: Stable carbon
496   isotopes of dissolved inorganic carbon in the Western North Pacific Ocean: Proxy for water mixing
497   and dynamics, Front. Mar. Sci., 9, http://doi.org/10.3389/fmars.2022.998437, 2022.

498   Guo, J., Zhou, B., Achterberg, E. P., Yuan, H., Song, J., Duan, L., and Li, X.: Rapid Cycling of Bacterial
499   Particulate Organic Matter in the Upper Layer of the Western Pacific Warm Pool, Geophys. Res.
500   Lett., 50, http://doi.org/10.1029/2023gl102896, 2023a.

501   Guo, J., Achterberg, E. P., Shen, Y., Yuan, H., Song, J., Liu, J., Li, X., and Duan, L.: Stable carbon isotopic
502   composition of amino sugars in heterotrophic bacteria and phytoplankton: Implications for
503   assessment of marine organic matter degradation, Limnology and Oceanography, 68, 2814-2825,
504   http://doi.org/10.1002/lno.12468, 2023b.

505   Häggi, C., Pätzold, J., Bouillon, S., and Schefuß, E.: Impact of selective degradation on molecular isotope
506   compositions   in   oxic   and   anoxic   marine   sediments,   Org.   Geochem.,   153,
507   http://doi.org/10.1016/j.orggeochem.2021.104192, 2021.

508   Hayes, J. M.: Factors controlling ^{13}C contents of sedimentary organic compounds: Principles and
509   evidence, Mar. Geol., 113, 111-125, http://doi.org/10.1016/0025-3227 (93)90153-m, 1993.

510   Henderson, L. C., Wittmers, F., Carlson, C. A., Worden, A. Z., and Close, H. G.: Variable carbon isotope
511   fractionation of photosynthetic communities over depth in an open-ocean euphotic zone, Proc Natl
512   Acad Sci U S A, 121, e2304613121, http://doi.org/10.1073/pnas.2304613121, 2024.

513   Herndl, G. J., Bayer, B., Baltar, F., and Reinthaler, T.: Prokaryotic Life in the Deep Ocean's Water Column,
514   Ann Rev Mar Sci, 15, 461-483, http://doi.org/10.1146/annurev-marine-032122-115655, 2023.

515   Hernes, P. J. and Benner, R.: Transport and diagenesis of dissolved and particulate terrigenous organic
516   matter in the North Pacific Ocean, Deep Sea Res. Part I Oceanogr. Res. Pap., 49, 2119-2132,
517   http://doi.org/10.1016/s0967-0637 (02)00128-0, 2002.

518   Hu, D., Wu, L., Cai, W., Gupta, A. S., Ganachaud, A., Qiu, B., Gordon, A. L., Lin, X., Chen, Z., Hu, S.,
519   Wang, G., Wang, Q., Sprintall, J., Qu, T., Kashino, Y., Wang, F., and Kessler, W. S.: Pacific western
520   boundary   currents   and   their   roles   in   climate,   Nature,   522,   299-308,
521   http://doi.org/10.1038/nature14504, 2015.

522   Hugler, M. and Sievert, S. M.: Beyond the Calvin cycle: autotrophic carbon fixation in the ocean, Ann
523   Rev Mar Sci, 3, 261-289, http://doi.org/10.1146/annurev-marine-120709-142712, 2011.

524   Hwang, J. and Druffel, E. R.: Lipid-like material as the source of the uncharacterized organic carbon in
525   the ocean?, Science, 299, 881-884, http://doi.org/10.1126/science.1078508, 2003.

526   Hwang, J., Druffel, E. R. M., Eglinton, T. I., and Repeta, D. J.: Source (s) and cycling of the
527   nonhydrolyzable organic fraction of oceanic particles, Geochim. Cosmochim. Acta, 70, 5162-5168,
528   http://doi.org/10.1016/j.gca.2006.07.020, 2006.

529   Iversen, M. H. and Ploug, H.: Temperature effects on carbon-specific respiration rate and sinking velocity
530   of diatom aggregates – potential implications for deep ocean export processes, Biogeosciences, 10,
531   4073-4085, http://doi.org/10.5194/bg-10-4073-2013, 2013.

532   Jeffrey, A. W. A., Pflaum, R. C., Brooks, J. M., and Sackett, W. M.: Vertical trends in particulate organic
533   carbon ^{13}C: ^{12}C ratios in the upper water column, Deep Sea Research Part A. Oceanographic
534   Research Papers, 30, 971-983, http://doi.org/10.1016/0198-0149 (83)90052-3, 1983.

Jia, Q., Li, T., Xiong, Z., Steinke, S., Jiang, F., Chang, F., and Qin, B.: Hydrological variability in the western tropical Pacific over the past 700 kyr and its linkage to Northern Hemisphere climatic change, Palaeogeogr. Palaeoclimatol. Palaeoecol., 493, 44-54, http://doi.org/10.1016/j.palaeo.2017.12.039, 2018.

Kharbush, J. J., Close, H. G., Van Mooy, B. A. S., Arnosti, C., Smittenberg, R. H., Le Moigne, F. A. C., Mollenhauer, G., Scholz-Böttcher, B., Obreht, I., Koch, B. P., Becker, K. W., Iversen, M. H., and Mohr, W.: Particulate Organic Carbon Deconstructed: Molecular and Chemical Composition of Particulate Organic Carbon in the Ocean, Front. Mar. Sci., 7, http://doi.org/10.3389/fmars.2020.00518, 2020.

Lee, C., Wakeham, S. G., and I. Hedges, J.: Composition and flux of particulate amino acids and chloropigments in equatorial Pacific seawater and sediments, Deep Sea Res. Part I Oceanogr. Res. Pap., 47, 1535-1568, http://doi.org/10.1016/s0967-0637 (99)00116-8, 2000.

Longhurst, A. R. and Glen Harrison, W.: The biological pump: Profiles of plankton production and consumption in the upper ocean, Prog. Oceanogr., 22, 47-123, http://doi.org/10.1016/0079-6611 (89)90010-4, 1989.

Ma, J., Song, J., Li, X., Yuan, H., Li, N., Duan, L., and Wang, Q.: Control factors of DIC in the Y3 seamount waters of the Western Pacific Ocean, J. Oceanol. Limnol., 38, 1215-1224, http://doi.org/10.1007/s00343-020-9314-3, 2020.

Ma, J., Song, J., Li, X., Wang, Q., Zhong, G., Yuan, H., Li, N., and Duan, L.: The OMZ and Its Influence on POC in the Tropical Western Pacific Ocean: Based on the Survey in March 2018, Front. Earth Sci., 9, http://doi.org/10.3389/feart.2021.632229, 2021.

Ma, J., Wen, L., Li, X., Dai, J., Song, J., Wang, Q., Xu, K., Yuan, H., and Duan, L.: Different fates of particulate matters driven by marine hypoxia: A case study of oxygen minimum zone in the Western Pacific, Mar. Environ. Res., 200, 106648, http://doi.org/10.1016/j.marenvres.2024.106648, 2024.

McCollom, T. M. and Amend, J. P.: A thermodynamic assessment of energy requirements for biomass synthesis by chemolithoautotrophic micro-organisms in oxic and anoxic environments, Geobiology, 3, 135-144, http://doi.org/10.1111/j.1472-4669.2005.00045.x, 2005.

Meyer, K. M., Ridgwell, A., and Payne, J. L.: The influence of the biological pump on ocean chemistry: implications for long-term trends in marine redox chemistry, the global carbon cycle, and marine animal ecosystems, Geobiology, 14, 207-219, http://doi.org/10.1111/gbi.12176, 2016.

Meyers, P. A.: Organic geochemical proxies of paleoceanographic, paleolimnologic, and paleoclimatic processes, Org. Geochem., 27, 213-250, http://doi.org/10.1016/s0146-6380 (97)00049-1, 1997.

Morales, M., Aflalo, C., and Bernard, O.: Microalgal lipids: A review of lipids potential and quantification for 95 phytoplankton species, Biomass and Bioenergy, 150, http://doi.org/10.1016/j.biombioe.2021.106108, 2021.

Owens, S. A., Pike, S., and Buesseler, K. O.: Thorium-234 as a tracer of particle dynamics and upper ocean export in the Atlantic Ocean, Deep Sea Res. Part II Top. Stud. Oceanogr., 116, 42-59, http://doi.org/10.1016/j.dsr2.2014.11.010, 2015.

Passos, J. G., Soares, L. F., Sumida, P. Y. G., Bendia, A. G., Nakamura, F. M., Pellizari, V. H., and Signori, C. N.: Contribution of chemoautotrophy and heterotrophy to the microbial carbon cycle in the Southwestern Atlantic Ocean, Ocean Coast. Res., 70, http://doi.org/10.1590/2675-2824070.22137jgp, 2022.

Quay, P. and Stutsman, J.: Surface layer carbon budget for the subtropical N. Pacific: constraints at station ALOHA, Deep Sea Res. Part I Oceanogr. Res. Pap., 50, 1045-1061, http://doi.org/10.1016/s0967-

579   0637 (03)00116-x, 2003.

580   Quay, P., Sonnerup, R., Munro, D., and Sweeney, C.: Anthropogenic CO_2 accumulation and uptake rates
581   in the Pacific Ocean based on changes in the $^{13}C/^{12}C$ of dissolved inorganic carbon, Glob.
582   Biogeochem. Cycles, 31, 59-80, http://doi.org/10.1002/2016gb005460, 2017.

583   Quay, P., Sonnerup, R., Westby, T., Stutsman, J., and McNichol, A.: Changes in the $^{13}C/^{12}C$ of dissolved
584   inorganic carbon in the ocean as a tracer of anthropogenic CO_2 uptake, Glob. Biogeochem. Cycles,
585   17, http://doi.org/10.1029/2001gb001817, 2003.

586   Radenac, M.-H., Messié, M., Léger, F., and Bosc, C.: A very oligotrophic zone observed from space in
587   the   equatorial   Pacific   warm   pool,   Remote   Sens.   Environ.,   134,   224-233,
588   http://doi.org/10.1016/j.rse.2013.03.007, 2013.

589   Reinthaler, T., van Aken, H. M., and Herndl, G. J.: Major contribution of autotrophy to microbial carbon
590   cycling in the deep North Atlantic's interior, Deep Sea Res. Part II Top. Stud. Oceanogr., 57, 1572-
591   1580, http://doi.org/10.1016/j.dsr2.2010.02.023, 2010.

592   Sannigrahi, P., Ingall, E. D., and Benner, R.: Cycling of dissolved and particulate organic matter at station
593   Aloha: Insights from ^{13}C NMR spectroscopy coupled with elemental, isotopic and molecular
594   analyses,   Deep   Sea   Res.   Part   I   Oceanogr.   Res.   Pap.,   52,   1429-1444,
595   http://doi.org/10.1016/j.dsr.2005.04.001, 2005.

596   Schmittner, A., Gruber, N., Mix, A. C., Key, R. M., Tagliabue, A., and Westberry, T. K.: Biology and air–
597   sea gas exchange controls on the distribution of carbon isotope ratios ($\delta^{13}C$) in the ocean,
598   Biogeosciences, 10, 5793-5816, http://doi.org/10.5194/bg-10-5793-2013, 2013.

599   Schönau, M. C., Rudnick, D. L., Gopalakrishnan, G., Cornuelle, B. D., and Qiu, B.: Mean, Annual, and
600   Interannual Circulation and Volume Transport in the Western Tropical North Pacific From the
601   Western   Pacific   Ocean   State   Estimates   (WPOSE),   J.   Geophys.   Res.   Oceans,   127,
602   http://doi.org/10.1029/2021jc018213, 2022.

603   Schouten, S., Klein Breteler, W. C. M., Blokker, P., Schogt, N., Rijpstra, W. I. C., Grice, K., Baas, M.,
604   and Sinninghe Damsté, J. S.: Biosynthetic effects on the stable carbon isotopic compositions of algal
605   lipids: implications for deciphering the carbon isotopic biomarker record, Geochim. Cosmochim.
606   Acta, 62, 1397-1406, http://doi.org/10.1016/s0016-7037 (98)00076-3, 1998.

607   Smith, C. R., De Leo, F. C., Bernardino, A. F., Sweetman, A. K., and Arbizu, P. M.: Abyssal food
608   limitation, ecosystem structure and climate change, Trends Ecol Evol, 23, 518-528,
609   http://doi.org/10.1016/j.tree.2008.05.002, 2008.

610   Song, J.: Biogeochemical Processes of Biogenic Elements in China Marginal Seas, Advanced Topics in
611   Science   and   Technology   in   China,   Springer   Berlin,   Heidelberg,   662   pp.,
612   http://doi.org/https://doi.org/10.1007/978-3-642-04060-3, 2010.

613   Sun, C., Xu, J., Liu, Z., Tong, M., and Zhu, B.: Application of Argo Data in the Analysis of Water Masses
614   in the Northwest Pacific Ocean, Marine Science Bulletin, 10, 2008.

615   Sun, Q., Song, J., Li, X., Yuan, H., and Wang, Q.: The bacterial diversity and community composition
616   altered in the oxygen minimum zone of the Tropical Western Pacific Ocean, J. Oceanol. Limnol.,
617   39, 1690-1704, http://doi.org/10.1007/s00343-021-0370-0, 2021.

618   Takahashi, T., Sutherland, S. C., Wanninkhof, R., Sweeney, C., Feely, R. A., Chipman, D. W., Hales, B.,
619   Friederich, G., Chavez, F., Sabine, C., Watson, A., Bakker, D. C. E., Schuster, U., Metzl, N.,
620   Yoshikawa-Inoue, H., Ishii, M., Midorikawa, T., Nojiri, Y., Körtzinger, A., Steinhoff, T., Hoppema,
621   M., Olafsson, J., Arnarson, T. S., Tilbrook, B., Johannessen, T., Olsen, A., Bellerby, R., Wong, C.
622   S., Delille, B., Bates, N. R., and de Baar, H. J. W.: Climatological mean and decadal change in

surface ocean pCO_2, and net sea–air CO_2 flux over the global oceans, Deep Sea Res. Part II Top. Stud. Oceanogr., 56, 554-577, http://doi.org/10.1016/j.dsr2.2008.12.009, 2009.

Thompson, R. O. R. Y.: Climatological Numerical Models of the Surface Mixed Layer of the Ocean, Journal of Physical Oceanography, 6, 496-503, 1976.

Tian, D., Li, X., Song, J., Ma, J, Yuan, H & Duan, L.: Vertical layering and transformation of Particulate organic carbon in the tropical Northwestern Pacific Ocean waters based on $\delta^{13}C$, Figshare [Dataset]. https://doi.org/10.6084/m9.figshare.26197808, 2024

Tuchen, F. P., Perez, R. C., Foltz, G. R., McPhaden, M. J., and Lumpkin, R.: Strengthening of the Equatorial Pacific Upper-Ocean Circulation Over the Past Three Decades, J. Geophys. Res. Oceans, 129, http://doi.org/10.1029/2024jc021343, 2024.

Turner, J. T.: Zooplankton fecal pellets, marine snow, phytodetritus and the ocean's biological pump, Prog. Oceanogr., 130, 205-248, http://doi.org/10.1016/j.pocean.2014.08.005, 2015.

Walsh, D. A., Zaikova, E., Howes, C. G., Song, Y. C., Wright, J. J., Tringe, S. G., Tortell, P. D., and Hallam, S. J.: Metagenome of a versatile chemolithoautotroph from expanding oceanic dead zones, Science, 326, 578-582, http://doi.org/10.1126/science.1175309, 2009.

Wu, L., Liu, Z., Liu, Y., Liu, Q., and Liu, X.: Potential global climatic impacts of the North Pacific Ocean, Geophys. Res. Lett., 32, http://doi.org/10.1029/2005gl024812, 2005.

Zeebe, R. E. and Wolf-Gladrow, D.: CO_2 in Seawater: Equilibrium, Kinetics, Isotopes, Elsevier Science, 2001.

Zhong, G., Li, X., Song, J., Qu, B., Wang, F., Wang, Y., Zhang, B., Tian, D., Ma, J., Yuan, H., Duan, L., Li, N., Wang, Q., and Xing, J.: The increasing big gap of carbon sink between the western and eastern Pacific in the last three decades, Front. Mar. Sci., 9, http://doi.org/10.3389/fmars.2022.1088181, 2022.

Zuo, J., Song, J., Yuan, H., Li, X., Li, N., and Duan, L.: Impact of Kuroshio on the dissolved oxygen in the East China Sea region, J. Oceanol. Limnol., 37, 513-524, http://doi.org/10.1007/s00343-019-7389-5, 2018.